



1 **Aerosol Optical Depth retrievals in Central Amazonia from a Multi-**
2 **Filter Rotating Shadow-band Radiometer on-site calibrated**

3

4 **Nilton E. Rosário¹, Tamara Sauini¹, Theotonio Pauliquevis¹, Henrique M. J. Barbosa²,**
5 **Marcia A. Yamasoe³, Boris Barja⁴**

6 ¹Universidade Federal de São Paulo - Rua São Nicolau 210 - Diadema - SP - CEP 09913-030 – Brazil

7 ²Instituto de Física da Universidade de São Paulo - Rua do Matão 1371 - São Paulo - SP - CEP 05508-090 - Brazil

8 ³Instituto de Astronomia, Geofísica e Ciências Atmosféricas - Universidade de São Paulo - Rua do Matão 1226 - São Paulo -
9 SP - CEP 05508-090 – Brazil

10 ⁴Universidade de Magallanes - Manuel Bulnes 01855, Punta Arenas, Region de Magallanes y de la Antártica Chilena, Chile

11 Correspondence to: Nilton E. Rosario (nrosario@unifesp.br)

12

13

Abstract

14 Extraterrestrial spectral response calibration of a Multi-Filter Rotating Shadow band Radiometer (MFRSR) under
15 Amazonian Forest atmosphere pristine conditions using the Langley plot method was performed and evaluated. The
16 MFRSR is installed in central Amazonia as part of a long-term monitoring site, which was used in the context of the
17 GoAmazon2014/5 Experiment. It has been operating continuously since 2011 without regular extraterrestrial
18 calibration, preventing its application to accurate monitoring of aerosol particles. Once calibrated, the MFRSR
19 measurements were applied to retrieve aerosols particles columnar optical properties, specifically Aerosol Optical
20 Depth (AOD_{λ}) and Ångström Exponent (AE), which were evaluated against retrievals from a collocated CIMEL
21 sunphotometer belonging to the AErosol RObotic NETwork (AERONET). Results obtained revealed that Amazonian
22 pristine conditions are able to provide MFRSR extraterrestrial spectral response with relative uncertainty lower than
23 1.0% at visible channels. The worst estimate (air mass = 1) for absolute uncertainty in AOD_{λ} retrieval varied from
24 ~ 0.02 to ~ 0.03 , depending on the assumption regarding uncertainty for MFRSR direct-normal irradiance measured
25 at the surface. Obtained Root Mean Square Errors (RMSE ~ 0.025) from the evaluation of MFRSR retrievals against
26 AERONET AOD_{λ} were, in general, lower than estimate MFRSR AOD_{λ} uncertainties, and close to AERONET field
27 sunphotometers (~ 0.02).



1 1. Introduction

2 Aerosol Optical Depth (AOD) is an important variable to characterize atmospheric particles
3 columnar abundance and is also fundamental to estimate their direct radiative forcing in the climate system
4 (Shaw, 1983, Kaufman et al. 2002, Menon, 2004, Satheesh and. Srinivasan, 2005). Its relevance is also
5 growing in the context of air quality monitoring from satellite (Hoff and Christopher, 2009, van Donkelaar
6 et al., 2010, van Donkelaar et al. 2013). However, the so called Extraterrestrial Response Calibration (ERC)
7 of the radiometers designed to monitor AOD, for instance sun tracking and shadow-band radiometers
8 (Holben et al., 1998, Harrison and Michalsky, 1994), is a critical issue to the accuracy of AOD retrievals
9 (O'Neill et al., 2005, Sinyuk et al., 2012, di Sarra et al., 2015). Therefore, regular and adequate calibration
10 of sun-tracking and shadow-band radiometers dedicated to monitor AOD is vital (Holben et al., 1998, Eck
11 et al., 1999, Michalsky et al., 2001). The ERC consists in the estimation of the solar energy that would be
12 measured by the instrument at the top of the atmosphere (TOA) or in hypothetical absence of the
13 atmosphere. It remains one of the most critical calibrations to the accuracy of AOD retrieval (Forgan, 1994;
14 Michalsky et al.; 2001, Eck et al., 1999; Chen et al., 2013). The classical way to perform ERC is based on
15 the Langley plot method, for which is recommended to take measurements on high mountains tops under
16 clean air and stable conditions (Shaw et al., 1976, Holben et al., 1998). However, very often, regular trip to
17 very high and clean mountain top to perform ERC are not possible, either due to the lack of resources or to
18 avoid data collection interruption. Consequently, with the spread of ground based AOD monitoring
19 networks, on site calibration based on multiple Langley plots has been successfully adopted elsewhere
20 (Michalsky et al., 2001, Augustine et al., 2008, Rosario et al., 2008, Mazzola et al., 2010, Michalsky et al.,
21 2013).

22 During the last decades, Amazonia has been a stage for various intensive and mid to long term
23 atmospheric experiments (Avisar et al., 2002, Silva Dias et al., 2002, Andreae et al., 2004, Martin et al.,
24 2016), performing a large number of field measurements, and regularly including ground-based monitoring
25 of AOD. Given the inherent complex logistics that characterize field experiments in Amazonia, regular trip
26 to distant clean mountain top to perform ERC of AOD monitoring devices operating inside the forest it is



1 a challenge, mainly for long-term sites. Unlike AEROSOL ROBOTIC NETWORK (AERONET) sunphotometers,
2 which have a regular calibration logistic supported by NASA (Holben et al., 1998), other ground-based
3 devices for AOD monitoring operating inside the Amazonia have to find alternative ways to provide regular
4 calibration. Multi-Filter Rotating Shadow-band Radiometers (MFRSR, Harrison and Michalsky, 1994) has
5 been also deployed recurrently in the Amazon basin to monitor spectral and broadband solar irradiance and
6 AOD during specific seasons (Yamasoe and Rosario, 2009, Rosario et al., 2009, Yamasoe et al., 2014,
7 Martin et al., 2016), and more recently focusing in mid and long-term monitoring (Barbosa et al., 2014).
8 An experimental site, located in central Amazonia, and included in the context of the Observations and
9 Modelling of the Green Ocean Amazon (GoAmazon2014/5, Martin et al., 2016) under the reference of T0e
10 is operating since the year of 2011 a MFRSR as part of a set of instruments to perform long term
11 atmospheric monitoring of convection, radiation, aerosols and cloud properties in central Amazonia
12 (Barbosa et al. 2014). GoAmazon experimental sites range from time point zero (T0) upwind of pollution
13 associated with Manaus city, Brazil (Figure 1) to sites in the midst (T1) and downwind (T2, T3) of the
14 pollution plume (Martin et al., 2016). The MFRSR is being operated in central Amazonia since 2011
15 without performing its ERC, which prevent its application to retrieve AOD. In this context, the question
16 that drives the focus of the present study is: Does Amazonia pristine atmosphere conditions provide
17 successful scenarios for Extraterrestrial Response Calibration? Amazonia atmosphere under pristine
18 conditions have been denominated as Green Ocean due to its very low pollution concentration, comparable
19 to remote ocean areas (Robert et al., 2001, Andreae et al., 2004), which is a fundamental requirement to
20 apply the Langley plot method. To answer the question posed, the present paper describes and discusses
21 methods and results of an effort to calibrate, on site, the cited MFRSR. Its subsequent application to
22 characterize the AOD variability is evaluated against AOD retrievals from a collocated Cimel
23 sunphotometer from AERONET (Holben et al., 1998). The manuscript is organized as follow: **section 2**
24 describes the experimental site, a brief overview on MFRSR and Langley plot method and AOD retrieval
25 theory, **section 3** consists of results and discussion and final remarks are exposed in **section 4**.

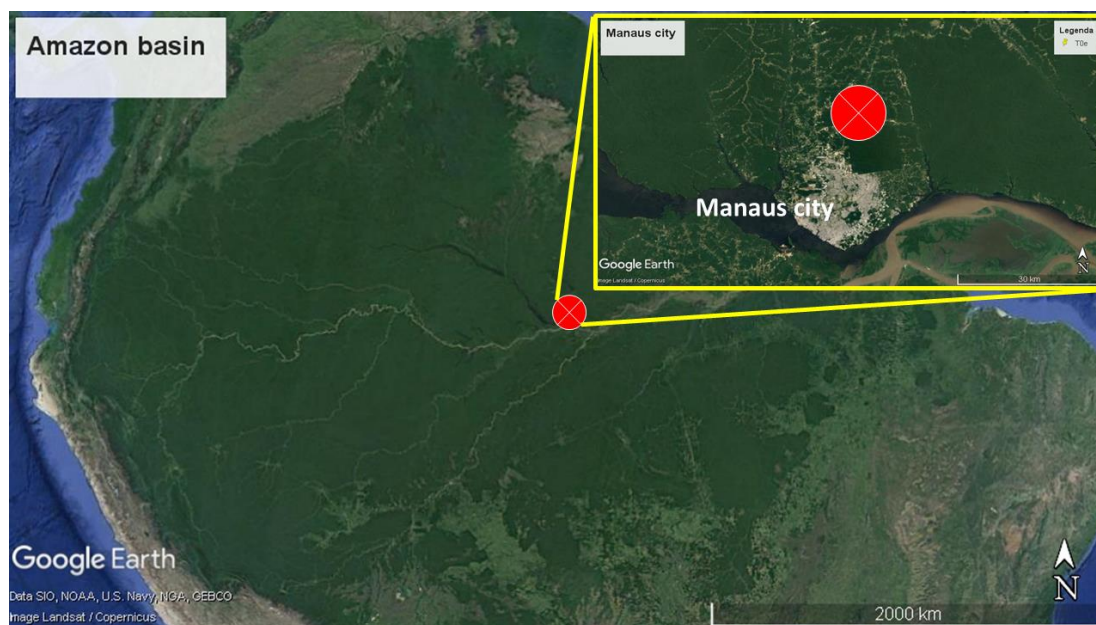
26



1 2. Experimental site, instruments, and methods

2 2.1 Experimental site T0e

3 The T0e site has been operating continuously since February 2011 in Central Amazonia, up-wind from
4 Manaus city ($59^{\circ} 58' 12''$ W and $02^{\circ} 53' 27''$ S, **Figure 1**), with a set of collocated atmospheric monitoring
5 instruments that include a MFRSR, a Cimel sunphotometer and a Raman lidar (Barbosa et al., 2014). The
6 site main goal is to provide long term characterization of diurnal and seasonal cycles of clouds and
7 convection and the interactions and feedback mechanisms between water vapour, clouds, radiation and
8 aerosol particles. It was incorporated as part of the GoAmazon 2014/15 experiment (Martin et al., 2016)
9 network sites, an international experiment designed to investigate the interactions that involve Amazonia
10 natural atmosphere conditions and the air pollution plume from Manaus city.



11 **Figure 1-** T0e site location in the Amazon basin and a zoom in showing the site location upwind of the Manaus City
(source: Google Earth maps).

12

13 The GoAmazon2014/5 sites were classified from time point zero (T0) upwind of the plume, to T1 in the
14 midst of the plume, to T2 just downwind of the Manaus, to T3 furthest downwind of Manaus (70 km).



1 During the wet season, the atmosphere at T0e site is a clean reference, since its location upwind of Manaus
2 prevents the site of being affected by the city pollution plume. Meanwhile, during the dry season the
3 atmospheric column at T0e, likewise large portion of atmosphere across central Amazonia, is influenced
4 by smoke from biomass burning emissions that occur throughout the Amazon basin.

5

6 **2.2 Instruments**

7 Multifilter Rotating Shadow-band Radiometer is designed to monitor global-horizontal, diffuse-
8 horizontal and direct-normal solar irradiances at narrow and broadband channels (Harrison et al., 1994). It
9 has been used worldwide to derive columnar aerosol optical properties (Harrison and Michalsky, 1994;
10 Alexandrov et al., 2002; Rosario et al., 2008, Michalsky et al., 2010, Mazzola et al., 2010, Michalsky and
11 LeBaron, 2013), water vapour (Michalsky et al, 1995, Alexandrov et al., 2009, Schneider et al, 2010) and
12 cloud optical properties (Min and Harrison, 1996, Wang and Min, 2008, Kassianov et al., 2011). Direct-
13 normal spectral irradiance ($I_{DN,\lambda}$) at the surface, needed to perform AOD retrievals, is obtained via the
14 difference between global-horizontal and diffuse-horizontal irradiances divided by the cosine of the solar
15 zenith angle (Harrison et al., 1994). Once MFRSR angular and spectral responses are properly characterized
16 and the automated shadow-band system adequately adjusted, accuracy in $I_{DN,\lambda}$ is expected to be comparable
17 to sunphotometers (Harrison et al., 1994). However, once in field, MFRSR filters transmission may suffer
18 degradation with time (Mychalsky et al, 2001, Michalsky and LeBaron, 2013), which makes regular ERC
19 critically necessary to keep the accuracy of AOD retrievals. The MFRSR of the present study has been
20 operating with sporadic interruptions at T0e providing irradiances measurements at time interval of 1
21 minute at five narrow-band channels (415, 500, 610, 670 and 870 nm) with half-bandwidth of 10 nm and
22 able to permit AOD retrieval. Given the high cloud cover in central Amazonia, the MFRSR high frequency
23 measurements are crucial to improve the frequency of AOD retrieval under cloudy sky and, therefore,
24 minimizes the AERONET known bias toward clear-sky condition (Levy et al., 2010).

25



1 2.3 Langley plot calibration and uncertainties

2 Langley plot calibration method is based on Lambert-Beer law (Shaw, 1983), which describes the
3 attenuation of a monochromatic beam propagating through a medium.

$$4 \quad I_{DN,\lambda} = f(d) I_{o,\lambda} e^{-m\tau_\lambda} \quad \text{eq. 1}$$

5 where, considering the full atmospheric column as a medium, $I_{DN,\lambda}$ is the direct solar spectral irradiance at
6 wavelength λ measured at the surface by the MFRSR, $I_{o,\lambda}$ is the solar spectral irradiance that would be
7 measured in the absence of the atmosphere at Earth-Sun mean distance (d_o), $f(d)$ is a correction factor
8 related to Earth-Sun distance variation (Iqbal, 1983), and m and τ_λ represent the atmosphere relative
9 optical air mass and total optical depth, respectively. Linearization of the equation 1 by applying the natural
10 logarithms to the both sides of the equation leads to a linear relation between m and $\ln(I_{DN,\lambda})$, on which
11 τ_λ and $\ln(f(d)I_{o,\lambda})$ represent, respectively, the angular and linear coefficients.

$$12 \quad \ln(I_{DN,\lambda}) = \ln(f(d)I_{o,\lambda}) - m\tau_\lambda \quad \text{eq. 2}$$

13 Knowing $\ln(I_{DN,\lambda})$ over a range of m , during which atmosphere remained clean and stable, the least-
14 squares regression method can be applied to provide a linear fit formulation between both variables, where
15 the angular coefficient is the mean atmosphere optical depth, and the linear coefficient represents the case
16 of m equal to zero, a hypothetical absence of atmosphere, from which an estimation of the solar
17 extraterrestrial spectral irradiance ($I_{o,\lambda}$) can be made.

18 In the present study, the atmosphere relative optical air mass (m) was calculated as a function of
19 Solar Zenith Angle (SZA) based on the Kasten and Young (1989) and $\ln(I_{DN,\lambda})$ taken from MFRSR direct-
20 normal irradiance measurements for the years of 2012 and 2015. As we assumed that both, the response
21 variable, $\ln(I_{DN,\lambda})$, and the predictor variable, m , are subject to errors, it was applied the least square
22 regression treatment that consider errors in both adjusted variables (Irvin and Quickenden, 1983). The errors
23 in $\ln(I_{DN,\lambda})$ were obtained through error propagation theory considering Harrison et al. (1994) estimate of
24 uncertainty to MFRSR direct-normal irradiance ($\sigma_{I_{DN,\lambda}} = 2\%$). Regarding error in the airmass (σ_m) we



1 based on the study of Tomasi and Petkov (2014), which compared atmospheric airmass results from Kasten
2 and Young (1989) formulation against rigorous calculation and found differences lower than 0.8%.
3 Therefore, we assume 0.8% as an estimate of uncertainty to the airmass calculated using Kasten and Young
4 (1989). Following previous studies suggestion (Mazzola et al., 2010 and Alexandrov et al., 2004), to apply
5 least square regression we adopted the airmass range from 2.0 to 5.0. For airmass larger than 5.0, high solar
6 energy incident angles, calibration may be affected due the uncertainty of the MFRSR cosine angle
7 correction and the shadow-band correction, meanwhile low airmasses, near 1.0, increase the probability of
8 turbulent atmospheric conditions and, therefore, the reduction of the optical depth stability (Chen et al.
9 2013).

10 The quality of the linear fit derived using least-square regression is highly dependent on optical depth
11 temporal stability, which is more likely to be observed under aerosol background conditions and stable
12 atmosphere. To obtain a set of linear fit able to provide high quality Langley plot calibration samples, for
13 both years 2012 and 2015, were selected only morning cases, to avoid the afternoon vigorous convection,
14 and only linear fit with correlation coefficients (R^2) higher than 0.990. This is the minimal value usually
15 obtained for calibration performed at high mountain top (Schmid and Wehrli, 1995). Also, considering
16 Schafer et al. (1998) study on AOD climatology across the Amazon basin, only AOD conditions typical of
17 background conditions were selected. For the both years studied, 2012 and 2015, the MFRSR final
18 extraterrestrial spectral response calibration ($\langle I_{o,\lambda} \rangle$) was estimated from the mean of the correspondent
19 set of extraterrestrial response calibration ($I_{o,\lambda}$) obtained from individual Langley plot calibrations. The
20 uncertainties of the derived final calibrations were estimate as the standard error of the mean ($\sigma_{\langle I_{o,\lambda} \rangle}$).
21 Subsequently, the final calibrations results were applied to retrieve AOD_λ over the Toe site using the
22 MFRSR.

23

24

25



1 2.4 Aerosol Optical Depth (AOD_λ) inversion and uncertainty estimate

2 From the eq. 2, the atmospheric total optical depth (τ_λ) can be separated as follow:

$$3 \quad \tau_{\lambda} = \tau_{m,\lambda} + AOD_{\lambda} + \tau_{g,\lambda} \quad \text{eq. 3}$$

4 Where τ_{m,λ}, τ_{g,λ} represent, respectively, molecular scattering and gas absorption optical depths. All
 5 MFRSR channels are affected by molecular scattering, while gas absorption is highly selective, therefore
 6 affects specific channels. The most relevant influence of gas absorption on MFRSR channels is produced
 7 by Ozone (O₃) at 610 and 670 nm channels and by Nitrogen Dioxide (NO₂) at 415 nm channel. Therefore,
 8 combination of the eq. 3 and eq. 2 leads to the AOD_λ retrieval equation

$$9 \quad AOD_{\lambda} = -\frac{1}{m} \ln \left[\frac{I_{DN,\lambda}}{f(d) < I_{o,\lambda} >} \right] - \tau_{m,\lambda} - \frac{m_{O_3}}{m} \tau_{O_3,\lambda} - \tau_{NO_2,\lambda} \quad \text{eq. 4}$$

10 where τ_{m,λ} was calculated using the Kasten and Young (1989) formulation as a function of the
 11 climatological surface atmospheric pressure. Given its unique vertical distribution, ozone relative optical
 12 air mass (m_{O₃}) was estimated separately based on Staehelin et al. (1995). Ozone and dioxide nitrogen
 13 absorption optical depths were obtained considering their spectral cross section absorption and average
 14 column content over the site, taken from the SCanning Imaging Absorption spectrOMeter for Atmospheric
 15 CHartography (SCIAMACHY, Bovensmann et al., 1999) and Ozone Monitoring Instrument (OMI, Levelt
 16 et al., 2006) products, respectively.

17 In general, the accuracy of the AOD_λ inversion is dominated by uncertainty in the extraterrestrial
 18 response calibration (< I_{o,λ} >) and I_{DN,λ} measurements (Michalsky et al., 2002, Alexandrov et al., 2007,
 19 Mazzola et al., 2010). Typically, uncertainties in both terms are at least one order of magnitude greater than
 20 the contributions of the other terms (Mazzola et al., 2010). Considering only the uncertainties in
 21 extraterrestrial response calibration (σ<I_{o,λ}>) and in I_{DN,λ} measurement (σ_{I_{DN,λ}}), an estimate of uncertainty
 22 (σ_{AOD_λ}) of the retrieved AOD_λ can be evaluated as

$$23 \quad \sigma_{AOD_{\lambda}} = \sqrt{\left[\frac{1}{m} \frac{\sigma_{<I_{o,\lambda}>}}{<I_{o,\lambda}>} \right]^2 + \left[\frac{1}{m} \frac{\sigma_{I_{DN,\lambda}}}{I_{DN,\lambda}} \right]^2} \quad \text{eq. 5}$$



1 where $\sigma_{\langle I_{0,\lambda} \rangle}$, as described, is based on the standard error of the mean of multiple extraterrestrial responses
2 obtained from a set of individual Langley plot calibration. Evaluation of the uncertainty in $I_{DN,\lambda}$ is a
3 challenge given its dependency on multiple factors, i.e., shadow-band adjustment, accuracy of the angular
4 response and MFRSR positioning regarding misalignment and tilt (Harrison et al., 1994, Alexandrov et al.,
5 2007). Harrison et al. (1994) estimated MFRSR $I_{DN,\lambda}$ typical uncertainty to vary between 2 and 3%.
6 Alexandrov et al. (2007) achieved lower estimation, roughly 1.5% for all channels. Assuming Harrison et
7 al. (1994) maximum uncertainty (3%), the final uncertainty in MFRSR AOD_{λ} , for all channels, was
8 evaluated for the worst case scenario, i.e., for unit relative air mass ($m = 1$).

9 Additionally, considering AOD_{λ} at two spectral channels (λ_1, λ_2) as reference, the spectral
10 dependence of AOD_{λ} was evaluated using Ångström exponent ($\alpha_{\lambda_1, \lambda_2}$), a parameter inversely related to
11 the average size of aerosol particles, calculated using the following equation

$$12 \quad \alpha_{\lambda_1, \lambda_2} = - \frac{\ln[AOD_{\lambda_1}/AOD_{\lambda_2}]}{\ln(\lambda_1/\lambda_2)} \quad \text{eq. 6}$$

13 Due to its dependency on aerosol size (Eck et al., 1999), $\alpha_{\lambda_1, \lambda_2}$ is a practical parameter to evaluate aerosol
14 particles size. High values of $\alpha_{\lambda_1, \lambda_2}$, greater than 1.5, indicate dominance of fine aerosol particles, while
15 values lower than 1.0 and close to zero are typically related to coarse aerosol particles dominance (Eck et
16 al., 1999). In central Amazonia, for regions up wind of urban areas, such as the T0e site, air masses rich in
17 fine aerosol particles are typically associated with smoke transport from biomass burning regions. Air
18 masses dominated by coarse particles fraction are in general associated with local and regional biogenic
19 and soil particles (Artaxo et al. 1998). Eventually, under favourable atmospheric circulation, air mass
20 containing coarse dust particles transported from Sahara Desert also may affect T0e site atmospheric
21 column (Koren et al., 2006, Ben-Ami et al., 2010).

22 Retrievals of AOD_{λ} and $\alpha_{\lambda_1, \lambda_2}$ from MFRSR measurements were validated against AERONET
23 direct Sun products Level 2.0 retrieved by a Cimel sunphotometer also installed at T0e site. AERONET
24 provides aerosol optical depth at seven wavelengths 340, 380, 440, 500, 670, 870 and 1020 nm, being three



1 coincident with MFRSR wavelengths, 500, 670 and 870 nm. In order to evaluate the MFRSR AOD_{λ} at the
2 remaining channels, 415 and 610 nm, the Ångström exponent from AERONET were used to perform
3 interpolation to derive AOD_{λ} in those channels for the network. Specifically for the comparison purpose,
4 MFRSR AOD_{λ} at 1 minute rate was averaged within a 5 minute interval centered on AERONET retrieval.
5 Large standard deviations from the mean were interpreted as cloud contamination in MFRSR, therefore
6 excluded from the analysis. Afterwards, MFRSR results were used to describe and analyse the seasonal
7 variability of columnar aerosol particles optical properties over T0e site.

8 The statistical metrics used to compare MFRSR AOD (AOD_{MFR}) with AERONET (AOD_{Aer}), assuming
9 the later as the true, are the root mean square error (RMSE), a measure of average deviation from the true,
10 and Bias, a measure of overall bias error or systematic error:

11

$$12 \quad RMSE = \sqrt{\frac{1}{N} \sum_{i=1}^N \left(\frac{AOD_{MFR,i} - AOD_{Aer,i}}{AOD_{Aer,i}} \right)^2} \quad eq.7$$

13

$$14 \quad Bias = \frac{1}{N} \sum_{i=1}^N \frac{AOD_{MFR,i} - AOD_{Aer,i}}{AOD_{Aer,i}} \quad eq.8$$

15

16

17

18

19

20

21

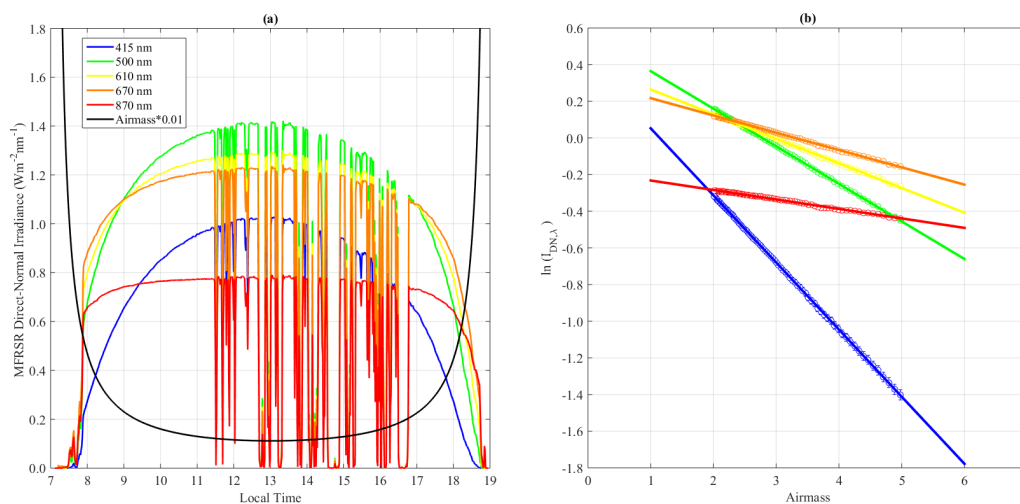


1 3. Results

2 3.1 MFRSR Langley plot calibration and uncertainty

3 An example of a the diurnal cycle of the spectral solar direct-normal irradiance measured (20 June
4 2012) by the MFRSR prone to a successful Langley plot is presented in **Figure 2**. In the morning period,
5 before vigorous convection initiate, the direct-normal irradiance at all channels is characterized by a
6 continuous increase. The suitability for a successful Langley plot is evidenced in the quality of the linear
7 fit achieved, as can be confirmed in **Table 1** for the 500 nm channel. **Table 1** and **Table 2** present for the
8 500 nm channels, respectively, for the years 2012 and 2015, the obtained extraterrestrial response
9 calibrations ($I_{o,\lambda}$) for each individual Langley plot that met the criteria defined, i.e. $R^2 \geq 0.990$ and
10 background AOD. The tables with the results for the remain channels (415, 610, 670 and 870 nm) are
11 presented in the supplementary material.

12



13

Figure 2 - (a) Diurnal cycle of air mass and global spectral solar irradiance measured by the MFRSR operating at the T0e site in Central Amazonia. (b) Example of Langley plot calibration applied to MFRSR spectral irradiance measurements taken under the clear sky period (08:00 to 11:00 Local Time) of the diurnal cycle shown in (a). (Day: 20 June 2012)

14



1 **Table 1** – Individual extraterrestrial calibration results ($I_{0,500\text{nm}}$) applying Langley Plot technique to measurements
 2 of solar direct-normal irradiance at 500 nm from a MFRSR operating at T0e site in Central Amazônia for the year
 3 2012. The individual uncertainty [$\sigma_{I_0\lambda}$] used to obtain the relative error [$\sigma_{I_0\lambda}$ (%)] was estimated from the
 4 **intercept** and its respective uncertainty ($\sigma_{\text{intercept}}$) derived from the least square regression method.

Date	slope	σ_{slope}	intercept	$\sigma_{\text{intercept}}$	$I_{0,500\text{ nm}}$	$\sigma_{I_0\lambda}$ (%)	R^2	N
17-may-12	-0.2426	0.0016	0.5709	0.0043	1.814	0.434	-0.9992	63
16-jun-12	-0.2450	0.0019	0.6058	0.0055	1.895	0.549	-0.9939	64
17-jun-12	-0.2237	0.0016	0.5560	0.0046	1.803	0.464	-0.9990	61
20-jun-12	-0.2117	0.0015	0.5846	0.0043	1.856	0.434	-0.9992	64
21-jun-12	-0.2261	0.0017	0.5722	0.0047	1.834	0.474	-0.9996	65
22-jun-12	-0.2265	0.0018	0.5362	0.0050	1.769	0.501	-0.9995	71
25-jun-12	-0.2585	0.0019	0.6461	0.0055	1.975	0.546	-0.9992	78
3-jul-12	-0.2493	0.0020	0.5848	0.0058	1.858	0.577	-0.9978	61
4-jul-12	-0.2436	0.0019	0.6060	0.0054	1.898	0.542	-0.9998	63
8-jul-12	-0.2430	0.0020	0.5668	0.0058	1.824	0.581	-0.9996	64
11-jul-12	-0.2420	0.0021	0.5456	0.0059	1.785	0.590	-0.9995	62
1-aug-12	-0.2616	0.0021	0.5843	0.0058	1.848	0.580	-0.9997	64
2-aug-12	-0.2401	0.0020	0.5221	0.0055	1.736	0.549	-0.9920	62
3-aug-12	-0.2775	0.0021	0.6313	0.0058	1.935	0.584	-0.9912	65
4-aug-12	-0.2359	0.0017	0.5751	0.0048	1.829	0.482	-0.9991	62
6-aug-12	-0.2880	0.0025	0.5561	0.0070	1.793	0.700	-0.9987	63
21-dec-12	-0.2658	0.0016	0.6294	0.0042	1.815	0.418	-0.9996	63

5

6 **Table 2** – Individual extraterrestrial calibration results ($I_{0,500\text{nm}}$) applying Langley Plot technique to measurements
 7 of solar direct-normal irradiance at 500 nm from a MFRSR operating at T0e site in Central Amazônia for the year
 8 2015. The individual uncertainty [$\sigma_{I_0\lambda}$] used to obtain the relative error [$\sigma_{I_0\lambda}$ (%)] was estimated from the
 9 **intercept** and its respective uncertainty ($\sigma_{\text{intercept}}$) derived from the least square regression method.

Date	slope	σ_{slope}	intercept	$\sigma_{\text{intercept}}$	$I_{0,500\text{ nm}}$	$\sigma_{I_0\lambda}$ (%)	R^2	N
19-feb-15	-0.2045	0.0014	0.5723	0.0041	1.734	0.412	-0.9959	62
27-mar-15	-0.2335	0.0015	0.5957	0.0039	1.809	0.395	-0.9941	69
4-jun-15	-0.2787	0.0021	0.6436	0.0058	1.963	0.583	-0.9923	68



24-jun-15	-0.1900	0.0013	0.5545	0.0039	1.802	0.394	-0.9996	63
1-jul-15	-0.2301	0.0016	0.6247	0.0048	1.933	0.478	-0.9989	62
2-jul-15	-0.2039	0.0015	0.5530	0.0043	1.800	0.433	-0.9995	62
6-jul-15	-0.2397	0.0019	0.6022	0.0054	1.890	0.542	-0.9979	61
10-jul-15	-0.2513	0.0019	0.6256	0.0055	1.934	0.546	-0.9988	61
11-jul-15	-0.2487	0.0019	0.6169	0.0056	1.917	0.556	-0.9996	61
12-jul-15	-0.2634	0.0022	0.5949	0.0063	1.876	0.634	-0.9993	61
15-jul-15	-0.2896	0.0026	0.6070	0.0074	1.898	0.745	-0.9994	61
28-jul-15	-0.2606	0.0020	0.6344	0.0056	1.945	0.555	-0.9982	62
29-jul-15	-0.2496	0.0021	0.5611	0.0059	1.807	0.585	-0.9901	62
30-jul-15	-0.2406	0.0018	0.5912	0.0051	1.862	0.510	-0.9964	62
1-aug-15	-0.2500	0.0019	0.6162	0.0054	1.908	0.536	-0.9954	62
2-aug-15	-0.2907	0.0024	0.6385	0.0066	1.950	0.657	-0.9983	62
7-aug-15	-0.2535	0.0018	0.6151	0.0051	1.902	0.508	-0.9997	64
23-aug-15	-0.2652	0.0018	0.6047	0.0048	1.870	0.482	-0.9987	69
5-sep-15	-0.2623	0.0018	0.5373	0.0044	1.737	0.438	-0.9983	74
9-sep-15	-0.2411	0.0014	0.6266	0.0038	1.895	0.376	-0.9996	75
22-sep-15	-0.2825	0.0018	0.5998	0.0045	1.831	0.454	-0.9992	75

1

2 The final extraterrestrial response estimations $\langle I_{o,\lambda} \rangle$, for both years and all channels, based on average
 3 of all individual Langley plot calibration, are presented in **Table 3** along the standard error from the mean
 4 as the uncertainty ($\sigma_{\langle I_{o,\lambda} \rangle}$), sample number (N) and the relative difference between calibration estimate
 5 for 2012 and 2015. The relative uncertainties among the channels varied from 0.7% (870 nm) to 1.0% (415
 6 nm) in 2012, and from 0.4% (870 nm) to 1.0% (415 nm) in 2015, which are surprisingly satisfactory for
 7 conditions diverse from those recommended (clean top mountain). Regarding the relative difference (-
 8 0.4%) between calibration constant derived for the two years, the difference for the channel 415 nm is not
 9 statistically significant, suggesting that between 2012 and 2015 the correspondent transmission filter did
 10 not suffer relevant degradation. Meanwhile, a drift of 4.8 % was observed for the 870 nm channel, an



1 indication of the lower stability of its transmission filter. The remain channels (500, 613, 670 nm)
 2 calibrations constant, opposite to the 870 nm channel, presented positive trend between 2012 and 2015
 3 calibrations. However, given the values of the uncertainty ($\sigma_{\langle I_{0,\lambda} \rangle}$) in their calibration constants, we are
 4 not able to attest that 500, 613 and 670 nm channels have statistically suffered degradation.

5 **Table 3** – MFRSR final extraterrestrial calibrations estimates $\langle I_{0,\lambda} \rangle$ for the years 2012 and 2015 averaging results
 6 of individual Langley plot calibration from Table 1, Table 2 and Tables in the supplementary material. The
 7 uncertainty estimation ($\sigma_{\langle I_{0,\lambda} \rangle}$) is based on the correspondent standard error of the average.

Channels	Year 2012			Year 2015			Difference (%)
	N	$\langle I_{0,\lambda} \rangle$	$\sigma_{\langle I_{0,\lambda} \rangle}$	N	$\langle I_{0,\lambda} \rangle$	$\sigma_{\langle I_{0,\lambda} \rangle}$	$\Delta \langle I_{0,\lambda} \rangle$ (2012-2015)
415 nm	21	1.586	0.015 (1.0 %)	22	1.579	0.017 (1.0%)	-0.4
500 nm	17	1.839	0.015 (0.8 %)	21	1.870	0.015 (0.8%)	+1.7
613 nm	14	1.545	0.010 (0.7%)	17	1.572	0.011 (0.7%)	+1.8
670 nm	15	1.416	0.010 (0.7%)	18	1.433	0.008 (0.6%)	+1.2
870 nm	15	0,842	0.008 (0.9%)	20	0.802	0.003 (0.4%)	-4.8

8

9 Considering the estimate uncertainties in the extraterrestrial calibration constant (0.4% -1.0%), and
 10 the Harrison et al. (1994) maximum uncertainty (3%) for MFRSR $I_{DN,\lambda}$ measurements, accordingly to the
 11 error propagation analysis (equation 6), the worst estimative (i.e., for unit airmass) for our absolute
 12 uncertainty in AOD_{λ} is ~ 0.03 , which is comparable with uncertainty of AOD_{λ} retrieved from AERONET
 13 field sunphotometers measurements (~ 0.02 , Eck et al., 1999). However, if a lower uncertainty in $I_{DN,\lambda}$ is
 14 assumed, for instance 1.5% (as suggested by Alexandrov et al., 2007), that would reduce MFRSR AOD_{λ}
 15 uncertainty from ~ 0.03 to ~ 0.02 .

16 In the general, perfect linear Langley plots are associated with stable aerosol optical depth, however
 17 it is possible that not all nearly linear Langley plots are able to provide correct calibration. Airmass
 18 assumption, mainly regarding aerosol particles airmass (Schmid and Wehrli, 1995), instruments induced
 19 artefact, the shadow-band system alignment (Chen et al., 2013), may contribute to error in calibration.

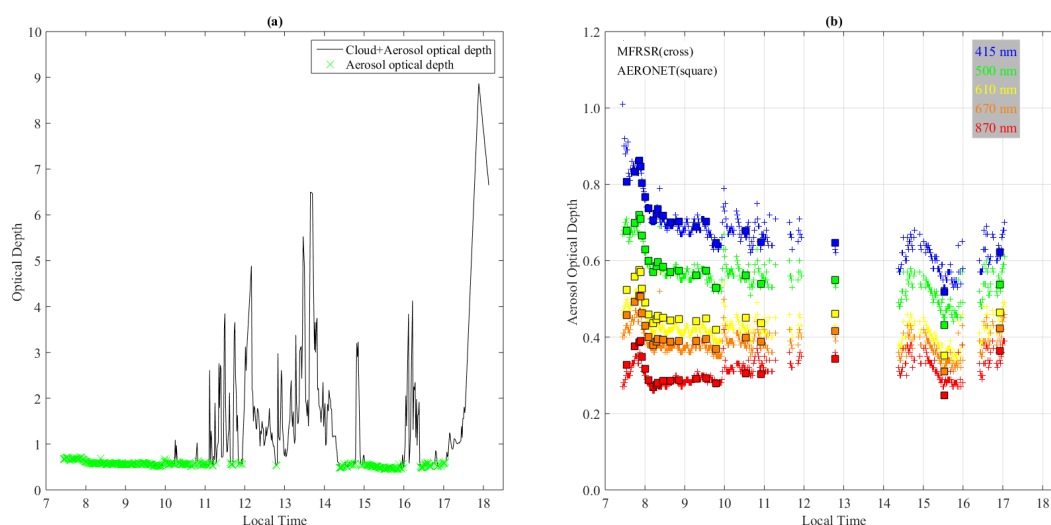


1 These influences are all challenge to estimate. Therefore, taking the mean of a set of individual Langley
2 plot calibration as the best estimate for the final calibration constant along the comparison of the AOD
3 results with AERONET retrieval should provide a good reference to evaluate the quality of the calibration
4 constant obtained. The results obtained for RMSEs derived from the comparison between MFRSR
5 retrievals and AERONET AOD are lower than the estimated uncertainty for MFRSR AOD_{λ} retrievals (i.e.,
6 $\sim 0.02 - 0.03$, depending on the $I_{\downarrow}(DN, \lambda)$ uncertainty assumed (1.5 or 3 %) and just above the maximum
7 uncertainty for AERONET field instrument (~ 0.02), demonstrating that, in spite of eventual error
8 associated with assumption made during the Langley plot application, the final derived constants are able
9 to provide reliable AOD retrievals.

10

11 **3.2 Aerosol Optical Depth (AOD_{λ}) inversion and uncertainty estimate**

12 Once determined the MFRSR channels final extraterrestrial response calibration, direct-normal
13 irradiance measurements taken along 2012 and 2015 were applied to retrieve AOD_{λ} and calculate
14 Ångström exponent. **Figure 3** illustrates, for a specific day (22 November 2012), results of cloud screening
15 and a comparison between the diurnal variability of AOD_{λ} from MFRSR and AERONET. The cloud
16 screening criteria captured the majority of contaminated measurements, but few suspicious remaining
17 points are likely related to optically thin cirrus. A more conservative algorithm would remove a significant
18 amount of cloud free cases, as seems to be the case for AERONET retrievals. The intercomparison showed
19 the consistency of MFRSR retrievals regarding AOD_{λ} diurnal variability. It is worth to emphasize the higher
20 frequency of MFRSR retrieval during the afternoon when compared with AERONET product. This is a
21 critical aspect regarding the representativity of AOD_{λ} diurnal variation in regions marked by strong diurnal
22 cycle of convection and cloud cover such as Central Amazonia. The MFRSR one minutes frequency is
23 expected to improve the statistic of AOD under cloudy conditions, since AERONET current statistics are
24 recognized to be biased toward cloudless sky conditions (Levy et al, 2010).



1

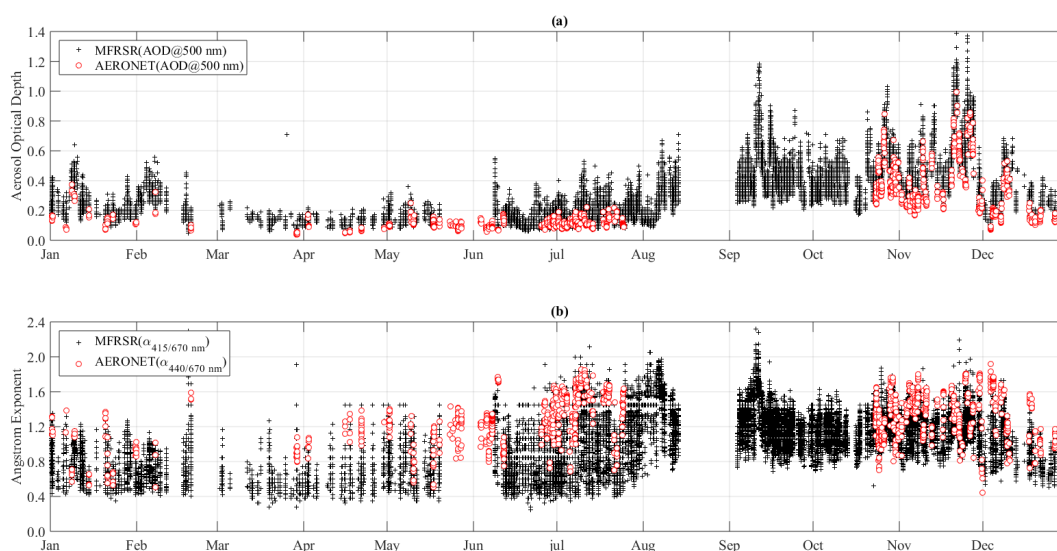
Figure 3 - (a) Example of the cloud screening applied to the MFRSR optical depth retrievals (22 November 2012). (b) Cloud screened diurnal cycle of multichannel aerosol optical depth from MFRSR compared with AOD retrievals from AERONET Level 2.0 product.

2

3 A comparison focusing on seasonal variability was also performed. **Figure 4** presents the 2012 seasonal
4 variability of $AOD_{500\text{ nm}}$ and $\alpha_{415,670\text{ nm}}$ over T0e site as seen by MFRSR (based on 1 min time resolution)
5 and AERONET. MFRSR retrievals were able to represent consistently the major seasonal features. From
6 March to June, central Amazonia presents its lowest $AOD_{500\text{ nm}}$ levels, ranging from ~ 0.05 to ~ 0.20 . In a
7 completely opposite scenario, during the biomass burning season (August to November), $AOD_{500\text{ nm}}$ hardly
8 goes down below 0.20 and values above 0.50 are quite frequent. During the transition periods, from
9 background conditions to biomass burning (June to July) and from biomass burning to background
10 (December to February), $AOD_{500\text{ nm}}$ values oscillated between typical background and biomass burning
11 season. Considering that the enhancement of AOD_{λ} during the biomass burning season across central
12 Amazonia is dominated by increase in small particles (Eck et al., 1999, Rosario, 2011), $\alpha_{415,670\text{ nm}}$
13 variability (**Figure 4**) is consistent with the AOD_{500} discussion, i. e., as the aerosol loading increase from
14 July to the biomass burning month (Aug-Sep-Oct-Nov), $\alpha_{415,670\text{ nm}}$ also shows an enhancement.
15 Ångström Exponents ranging from 0.4 to 0.8, which are dominant under background conditions, became



1 rare throughout the biomass burning season and intermittent during the transition periods, a feature
2 consistently described by MFRSR and AERONET. Similar results, for both AOD_{500} and $\alpha_{415,670\text{ nm}}$
3 were observed regarding the year 2015 (not shown here).



4

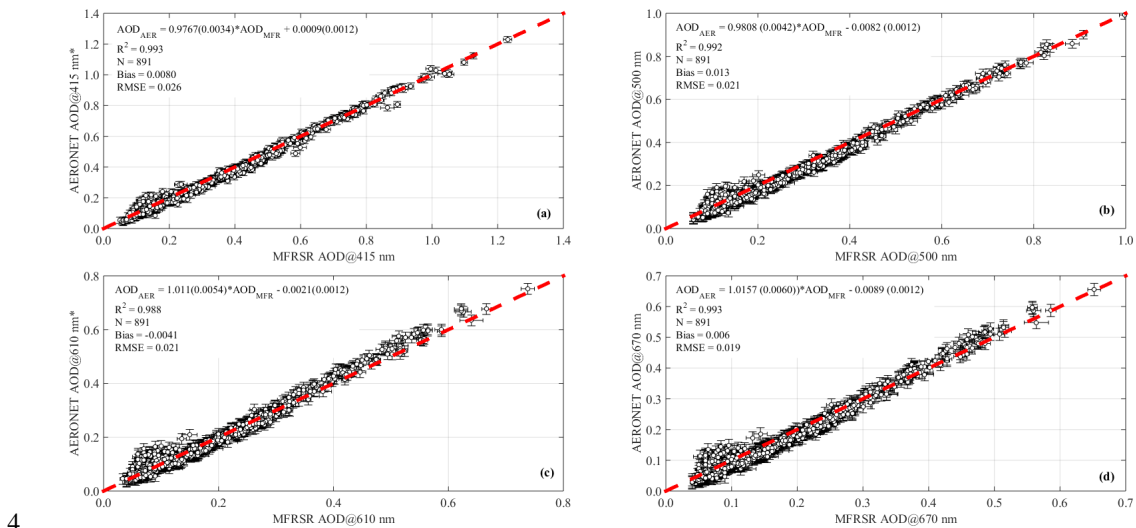
Figure 4 – (a) Seasonal aerosol optical Depth and (b) Angstrom exponent variability in Central Amazonia as obtained via the on-site calibrated MFRSR (this study) and the AERONET sunphotometer for the year 2012.

5

6 **Figures 5** and **6** show scatter plots and statistic metrics (Bias, RMSE and Correlation coefficient)
7 comparing MFRSR and AERONET retrievals for 2012 and 2015, respectively. In general, there is a good
8 agreement between both AOD_{λ} retrievals. However, non-negligible trends are seen, especially for 2012,
9 and in particular for the lower and higher AOD_{λ} values. For low AOD_{λ} values, a systematic underestimation
10 by MFRSR is observed for all channels, while for high AOD_{λ} , the longer wavelength channels (610 and
11 670 nm) tend to underestimate aerosol optical depth. For the 2015 years trends are less evident, mainly for
12 the low aerosol loading when compared with 2012. Nevertheless, overall, the statistics metrics (**Table 4**)
13 used to evaluate MFRSR retrievals performance against AERONET suggest that, when is not possible to
14 perform high top mountain calibration, the extraterrestrial response calibration performed at Central



- 1 Amazonia has reliability to support consistent retrievals of aerosol optical depth. The obtained RMSEs are
- 2 lower than the estimated uncertainty for MFRSR AOD_{λ} retrievals (i.e., $\sim 0.02 - 0.03$, depending on the $I_{DN,\lambda}$
- 3 uncertainty assumed) and just above the maximum uncertainty for AERONET field instrument (~ 0.02).



4

Figure 5 - Spectral AOD retrieval from the on-site calibrated MFRSR as a function of AOD from AERONET direct product level 2.0 for the year 2012.

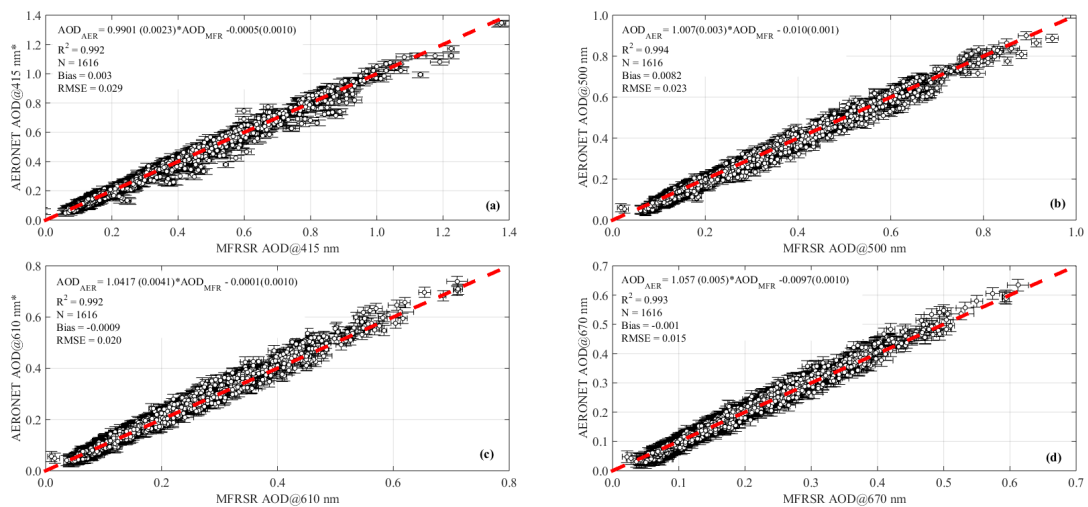


Figure 6 - Spectral AOD retrieval from the on-site calibrated MFRSR as a function of AOD from AERONET direct product level 2.0 for the year 2015.

5



1 **Table 4** – Summary of the statistical metrics used to evaluate MFRSR aerosol optical depth (X) against AERONET
 2 optical depth (Y) for the coincident spectral channels (500, 670 and 870 nm): Bias, Root Mean Square Error (RMSE).
 3 The linear fit regression parameters, slope (A) and intercept (B) and correspondent uncertainty (σ_A ; σ_B) are also
 4 presented.

	λ	N	Bias	RMSE	$Y = A (\sigma_A) * X + B (\sigma_B)$	R^2
2012	500 nm	891	0.0130	0.021	A = 0.9808 (0.0042); B = -0.0082 (0.0012)	0.992
	670 nm	891	0.0064	0.019	A = 1.0157 (0.0060); B = -0.0089 (0.0012)	0.988
	870 nm	891	0.0148	0.031	A = 0.901 (0.007); B = -0.0016 (0.0012)	0.962
2015	500 nm	1616	0.0082	0.023	A = 1.007 (0.003); B = -0.010 (0.001)	0.994
	670 nm	1616	-0.0010	0.015	A = 1.057 (0.005); B = -0.0097 (0.0010)	0.993
	870 nm	1616	-0.0040	0.016	A = 1.1285 (0.0073); B = -0.0136 (0.0011)	0.9895

5

6 **4. Conclusions**

7 Do Central Amazonian pristine atmosphere provides successful extraterrestrial response calibration based
 8 on Langley plot method? This question emerged from the challenge to maintain regular calibration of a
 9 MFRSR dedicated to long-term retrieval of columnar aerosol optical properties in central Amazônia. To
 10 answer the question, the MFRSR was calibrated on site using the Langley plot method for two distinct
 11 years, 2012 and 2015, and subsequently applied to retrieve aerosol columnar optical properties, i.e., Aerosol
 12 Optical Depth (AOD) and Ångström Exponent (AE). Retrievals were evaluated against direct sun inversion
 13 products (Level 2.0) from a collocated sunphotometer belonging to AERONET. Results obtained show that
 14 on site calibration using Langley plot, under Amazonian pristine conditions, is able to provide
 15 extraterrestrial response with relative uncertainties varying from ~0.4 to ~1.0 % at MFRSR visible channels.
 16 The worst estimative (airmass = 1) for absolute uncertainty in retrieved AOD_λ can varied from ~0.03 to
 17 ~0.02, depending on the assumption regarding the uncertainty assumed for MFRSR direct-normal
 18 irradiance measured at the surface ($I_{DN,\lambda}$), which in the literature varied from 1.5% to 3.0%. All Root
 19 Mean Square Error (RMSE), obtained from the comparison of MFRSR retrievals against AERONET AOD_λ
 20 for coincident channels (500 and 670 nm), were lower (< 0.025) than the estimated MFRSR AOD_λ



1 uncertainties and close to AERONET field sunphotometers (~ 0.02). Under the point of view of the question
2 posed, these results suggest that on site calibration in central Amazonia pristine conditions is able to provide
3 consistent retrieval of AOD_{λ} . Another relevant aspect of the results provided by the MFRSR, due to its high
4 measurement frequency (one minute), is the improvement of the statistic of AOD under cloudy conditions,
5 which is critical for Amazonia. AERONET current statistics are expected to be biased to cloudless sky
6 conditions, which are dominant during the morning period and dry season.

7 **Competing interests.** The authors declare that there are no competing interests

8 **Acknowledgements.** The authors would like to EMBRAPA, INPA, and the LBA Central office for
9 logistical support. Special thanks to Marcelo Rossi, Victor Souza, and Jocivaldo Souza at EMBRAPA, and
10 to Ruth Araujo, Roberta Souza, Bruno Takeshi, and Glauber Cirino from LBA. Henrique Barbosa
11 acknowledges the financial support from FAPESP Research Program on Global Climate Change under
12 research grants 2008/58100-1, 2012/16100-1, 2013/50510-5, and 2013/05014-0. Theotonio Pauliquevis
13 acknowledges the financial support from CNPq research grant 458017/2013-2. Boris Barja acknowledges
14 the financial support of CAPES project A016_2013 on the program Science without Frontiers and the
15 SAVERNET project.



1 References

- 2 Alexandrov, M. D., Lacis, A. A., Carlson, B. E., and Cairns, B.: Remote Sensing of Atmospheric Aerosols
3 and Trace Gases by Means of Multifilter Rotating Shadowband Radiometer. Part II: Climatological
4 Applications, *Journal of the Atmospheric Sciences*, 59, 544–566, [https://doi.org/10.1175/1520-](https://doi.org/10.1175/1520-0469(2002)059<0544:RSOAAA>2.0.CO;2)
5 [0469\(2002\)059<0544:RSOAAA>2.0.CO;2](https://doi.org/10.1175/1520-0469(2002)059<0544:RSOAAA>2.0.CO;2), 2002.
- 6
- 7 Alexandrov, M. D., Kiedron, P., Michalsky, J. J., Hodges, G., Flynn, C. J., and Lacis, A. A.: Optical depth
8 measurements by shadow-band radiometers and their uncertainties, *Appl. Opt.*, 46, 8027–8038,
9 <https://doi.org/10.1364/AO.46.008027>, 2007.
- 10
- 11 Andreae, M. O., Rosenfeld, D., Artaxo, P., Costa, A. A., Frank, G. P., Longo, K. M., and Silva-Dias, M.
12 A. F.: Smoking Rain Clouds over the Amazon, *Science*, 303, 1337–1342,
13 <https://doi.org/10.1126/science.1092779>, 2004.
- 14
- 15 Artaxo, P., Fernandes, E. T., Martins, J. V., Yamasoe, M. A., Hobbs, P. V., Maenhaut, W., Longo, K. M.,
16 and Castanho, A.: 10 Large-scale aerosol source apportionment in Amazonia, *Journal of Geophysical*
17 *Research: Atmospheres*, 103, 31 837–31 847, <https://doi.org/10.1029/98JD02346>, 1998.
- 18
- 19 Augustine, J. A., Hodges, G. B., Dutton, E. G., Michalsky, J. J., and Cornwall, C. R.: An aerosol optical
20 depth climatology for NOAA’s national surface radiation budget network (SURFRAD), *Journal of*
21 *Geophysical Research: Atmospheres*, 113, n/a–n/a, <https://doi.org/10.1029/2007JD009504>, d11204, 2008.
- 22
- 23 Avissar, R., Silva Dias, P. L., Silva Dias, M. A. F., and Nobre, C.: The Large-Scale Biosphere-Atmosphere
24 Experiment in Amazonia(LBA): Insights and future research needs, *Journal of Geophysical Research:*
25 *Atmospheres*, 107, LBA 54–1–LBA 54–6, <https://doi.org/10.1029/2002JD002704>, 8086, 2002.
- 26
- 27 Barbosa, H. M. J., Barja, B., Pauliquevis, T., Gouveia, D. A., Artaxo, P., Cirino, G. G., Santos, R. M. N.,
28 and Oliveira, A. B.: A permanente Raman lidar station in the Amazon: description, characterization, and
29 first results, *Atmospheric Measurement Techniques*, 7, 1745–1762, 20 [https://doi.org/10.5194/amt-7-1745-](https://doi.org/10.5194/amt-7-1745-2014)
30 [2014](https://doi.org/10.5194/amt-7-1745-2014), 2014.
- 31
- 32 Ben-Ami, Y., Koren, I., Rudich, Y., Artaxo, P., Martin, S. T., and Andreae, M. O.: Transport of North
33 African dust from the Bodélé depression to the Amazon Basin: a case study, *Atmospheric Chemistry and*
34 *Physics*, 10, 7533–7544, <https://doi.org/10.5194/acp-10-7533-2010>, 2010.
- 35
- 36 Bovensmann, H., Burrows, J. P., Buchwitz, M., Frerick, J., Noël, S., Rozanov, V. V., Chance, K. V., and
37 Goede, A. P. H.: SCIAMACHY: Mission Objectives and Measurement Modes, *Journal of the Atmospheric*
38 *Sciences*, 56, 127–150, [https://doi.org/10.1175/1520-](https://doi.org/10.1175/1520-0469(1999)056<0127:SMOAMM>2.0.CO;2)
39 [0469\(1999\)056<0127:SMOAMM>2.0.CO;2](https://doi.org/10.1175/1520-0469(1999)056<0127:SMOAMM>2.0.CO;2),
1999.
- 40
- 41 Chen, M., Davis, J., Tang, H., Ownby, C., and Gao, W.: The calibration methods for Multi-Filter Rotating
42 Shadowband Radiometer: a review, *Frontiers of Earth Science*, 7, 257–270,
43 <https://doi.org/10.1007/s11707-013-0368-9>, 2013.



1

2 di Sarra, A., Sferlazzo, D., Meloni, D., Anello, F., Bommarito, C., Corradini, S., Silvestri, L. D., Iorio, T.
3 D., Monteleone, F., Pace, G., Piacentino, S., and Pugnaghi, S.: Empirical correction of multifilter rotating
4 shadowband radiometer (MFRSR) aerosol optical depths for the aerosol forward scattering and
5 development of a long-term integrated MFRSR-Cimel dataset at Lampedusa, *Appl. Opt.*, 54, 2725– 2737,
6 <https://doi.org/10.1364/AO.54.002725>, 2015.

7

8 Eck, T. F., Holben, B. N., Reid, J. S., Dubovik, O., Smirnov, A., O'Neill, N. T., Slutsker, I., and Kinne, S.:
9 Wavelength dependence of the optical depth of biomass burning, urban, and desert dust aerosols, *Journal*
10 *of Geophysical Research: Atmospheres*, 104, 31 333–31 349, <https://doi.org/10.1029/1999JD900923>,
11 1999.

12

13 Forgan, B. W.: General method for calibrating Sun photometers, *Appl. Opt.*, 33, 4841–4850,
14 <https://doi.org/10.1364/AO.33.004841>, 1994.

15

16 Gueymard, C. A.: Interdisciplinary applications of a versatile spectral solar irradiance model: A review,
17 *Energy*, 30, 1551 – 1576, <https://doi.org/https://doi.org/10.1016/j.energy.2004.04.032>, measurement and
18 Modelling of Solar Radiation and Daylight- Challenges for the 21st Century, 2005.

19

20 Harrison, L. and Michalsky, J.: Objective algorithms for the retrieval of optical depths from ground-based
21 measurements, *Appl. Opt.*, 33, 5 5126–5132, <https://doi.org/10.1364/AO.33.005126>, 1994.

22

23 Harrison, L., Michalsky, J., and Berndt, J.: Automated multifilter rotating shadow-band radiometer: an
24 instrument for optical depth and radiation measurements, *Appl. Opt.*, 33, 5118–5125,
25 <https://doi.org/10.1364/AO.33.005118>, 1994.

26

27 Hoff, R. M. and Christopher, S. A.: Remote Sensing of Particulate Pollution from Space: Have We Reached
28 the Promised Land?, *Journal of the Air & Waste Management Association*, 59, 645–675,
29 <https://doi.org/10.3155/1047-3289.59.6.645>, 2009.

30 10 Holben, B., Eck, T., Slutsker, I., Tanré, D., Buis, J., Setzer, A., Vermote, E., Reagan, J., Kaufman, Y.,
31 Nakajima, T., Lavenu, F., Jankowiak, I., and Smirnov, A.: AERONET—A Federated Instrument Network
32 and Data Archive for Aerosol Characterization, *Remote Sensing of Environment*, 66, 1 – 16,
33 [https://doi.org/https://doi.org/10.1016/S0034-4257\(98\)00031-5](https://doi.org/https://doi.org/10.1016/S0034-4257(98)00031-5), 1998.

34

35 Iqbal, M.: *An Introduction to Solar Radiation*, Academic Press, San Diego, California, 1983.

36

37 Irvin, J. A. and Quickenden, Terry I. Linear least squares treatment when there are errors in both x and y.
38 *Journal of Chemical Education* 1983 60 (9), 711 DOI: 10.1021/ed060p711

39

40 Kassianov, E., Barnard, J., Berg, L. K., Long, C. N., and Flynn, C.: Shortwave spectral radiative forcing of
41 cumulus clouds from surface observations, *Geophysical Research Letters*, 38, n/a–n/a,
42 <https://doi.org/10.1029/2010GL046282>, 107801, 2011.

43



- 1 Kasten, F. and Young, A. T.: Revised optical air mass tables and approximation formula, *Appl. Opt.*, 28,
2 4735–4738,
3 <https://doi.org/10.1364/AO.28.004735>, 1989.
4
- 5 Kaufman, Y. J., Tanre, D., and Boucher, O.: A satellite view of aerosols in the climate system, *Nature*, 419,
6 215–223, 2002.
7
- 8 Koren, I., Kaufman, Y. J., Washington, R., Todd, M. C., Rudich, Y., Martins, J. V., and Rosenfeld, D.: The
9 Bodélé depression: a single spot in the Sahara that provides most of the mineral dust to the Amazon forest,
10 *Environmental Research Letters*, 1, 014 005, 2006.
11
- 12 Levelt, P. F., van den Oord, G. H. J., Dobber, M. R., Malkki, A., Visser, H., de Vries, J., Stammes, P.,
13 Lundell, J. O. V.,
14 and Saari, H.: The ozone monitoring instrument, *IEEE Transactions on Geoscience and Remote Sensing*,
15 44, 1093–1101, <https://doi.org/10.1109/TGRS.2006.872333>, 2006.
16
- 17 Levy, R. C., Remer, L. A., Kleidman, R. G., Mattoo, S., Ichoku, C., Kahn, R., and Eck, T. F.: Global
18 evaluation of the Collection 5 MODIS dark-target aerosol products over land, *Atmospheric Chemistry and
19 Physics*, 10, 10 399–10 420, <https://doi.org/10.5194/acp-10-10399-2010>, 2010.
20
- 21 Martin, S. T., Artaxo, P., Machado, L. A. T., Manzi, A. O., Souza, R. A. F., Schumacher, C., Wang, J.,
22 Andreae, M. O., Barbosa, H. M. J., Fan, J., Fisch, G., Goldstein, A. H., Guenther, A., Jimenez, J. L., Pöschl,
23 U., Silva Dias, M. A., Smith, J. N., and Wendisch, M.: Introduction: Observations and Modeling of the
24 Green Ocean Amazon (GoAmazon2014/5), *Atmospheric Chemistry and Physics*, 16, 4785–4797,
25 <https://doi.org/10.5194/acp-16-4785-2016>, 2016.
26
- 27 Mazzola, M., Lanconelli, C., Lupi, A., Busetto, M., Vitale, V., and Tomasi, C.: Columnar aerosol optical
28 properties in the Po Valley, Italy, from MFRSR data, *Journal of Geophysical Research: Atmospheres*, 115,
29 n/a–n/a, <https://doi.org/10.1029/2009JD013310>, d17206, 2010.
30
- 31 Menon, S.: Current Uncertainties In Assessing Aerosol Effects On Climate, *Annual Review of Environment
32 and Resources*, 29, 1–30, <https://doi.org/10.1146/annurev.energy.29.063003.132549>, 2004.
33
- 34 Michalsky, J. and LeBaron, B.: Fifteen-year aerosol optical depth climatology for Salt Lake City, *Journal
35 of Geophysical Research: Atmospheres*, 118, 3271–3277, <https://doi.org/10.1002/jgrd.50329>, 2013.
36
- 37 Michalsky, J., Denn, F., Flynn, C., Hodges, G., Kiedron, P., Koontz, A., Schlemmer, J., and Schwartz, S.
38 E.: Climatology
39 of aerosol optical depth in north-central Oklahoma: 1992–2008, *Journal of Geophysical Research:
40 Atmospheres*, 115,
41 <https://doi.org/10.1029/2009JD012197>, d07203, 2010.
42



- 1 Michalsky, J. J., Liljegren, J. C., and Harrison, L. C.: A comparison of Sun photometer derivations of total
2 column water vapor and ozone to standard measures of same at the Southern Great Plains Atmospheric
3 Radiation Measurement site, *Journal of Geophysical Research: Atmospheres*, 100, 25 995–26 003,
4 <https://doi.org/10.1029/95JD02706>, 1995.
- 5
- 6 Michalsky, J. J., Schlemmer, J. A., Berkheiser, W. E., Berndt, J. L., Harrison, L. C., Laulainen, N. S.,
7 Larson, N. R., and Barnard, J. C.: Multiyear measurements of aerosol optical depth in the Atmospheric
8 Radiation Measurement and Quantitative Links programs, *Journal of Geophysical Research: Atmospheres*,
9 106, 12 099–12 107, <https://doi.org/10.1029/2001JD900096>, 2001.
- 10
- 11 Min, Q. and Harrison, L. C.: Cloud properties derived from surface MFRSR measurements and comparison
12 with GOES results at the ARM SGP Site, *Geophysical Research Letters*, 23, 1641–1644,
13 <https://doi.org/10.1029/96GL01488>, 1996.
- 14
- 15 O’Neill, N. T., McArthur, L. J. B., and Strawbridge, K. B.: Recent progress in the remote sensing of
16 aerosols, *Physics in Canada, Special issue on Planetary Remote Sensing in Canada*, 61, 235–241, 2005.
- 17 Roberts, G. C., Andreae, M. O., Zhou, J., and Artaxo, P.: Cloud condensation nuclei in the Amazon Basin:
18 “marine” conditions over a continent?, *Geophysical Research Letters*, 28, 2807–2810,
19 <https://doi.org/10.1029/2000GL012585>, 2001.
- 20
- 21 Rosario, N.: Variability of aerosol optical properties over South America and the impacts of direct radiative
22 effect of aerosols from biomass burning, Ph.D. thesis, Institute of Astronomy, Geophysics and Atmospheric
23 Sciences, University of São Paulo, 2011.
- 24
- 25 Rosario, N., Yamasoe, M. A., Sayao, A., and Siqueira, R.: Multifilter rotating shadowband radiometer
26 calibration for spectral aerosol optical depth retrievals over Sao Paulo City, Brazil, *Appl. Opt.*, 47, 1171–
27 1176, <https://doi.org/10.1364/AO.47.001171>, 2008.
- 28
- 29 Rosario, N. E., Yamasoe, M. A., and Longo, K. M.: Aerosol Optical Depth and Ångström Coefficient
30 retrievals over the Amazon Forest during 2007 biomass burning season, *AIP Conference Proceedings*,
31 1100, 494–497, <https://doi.org/10.1063/1.3117029>, 2009.
- 32
- 33 Satheesh, S. K. and Srinivasan, J.: A method to infer short wave absorption due to aerosols using satellite
34 remote sensing, *Geophysical Research Letters*, 32, <https://doi.org/10.1029/2005GL023064>, 113814, 2005.
- 35
- 36 Schafer, J. S.; T. F. Eck; B. N. Holben; P. Artaxo; A. F. Duarte, 2008: Characterization of the optical
37 properties of atmospheric aerosols in Amazonia from long-term AERONET monitoring (1993-1995 and
38 1999-2006). *Journal of Geophysical Research: Atmospheres*, 113, D04204,
39 <https://doi.org/10.1029/2007JD009319>
- 40
- 41 Schmid, B., and C. Wehrli, Comparison of the sun photometer calibration by use of the Langley technique
42 and the standard lamp, *Appl. Opt.*, 34, 4500–4512, 1995.
- 43



- 1 Schneider, M., Romero, P. M., Hase, F., Blumenstock, T., Cuevas, E., and Ramos, R.: Continuous quality
2 assessment of atmospheric water vapour measurement techniques: FTIR, Cimel, MFRSR, GPS, and
3 Vaisala RS92, *Atmospheric Measurement Techniques*, 3, 323–338, [https://doi.org/10.5194/amt-3-323-](https://doi.org/10.5194/amt-3-323-2010)
4 2010, 2010.
- 5
- 6 Shaw, G. E.: Sun Photometry, *Bulletin of the American Meteorological Society*, 64, 4–10,
7 [https://doi.org/10.1175/1520-0477\(1983\)064<0004:SP>2.0.CO;2](https://doi.org/10.1175/1520-0477(1983)064<0004:SP>2.0.CO;2), 1983.
- 8
- 9 Shaw, G. E., Reagan, J. A., and Herman, B. M.: Investigations of Atmospheric Extinction Using Direct
10 Solar Radiation Measurements Made with a Multiple Wavelength Radiometer, *Journal of Applied*
11 *Meteorology* (1962-1982), 12, 374–380, 1973.
- 12
- 13 Silva Dias, M. A. F., Rutledge, S., Kabat, P., Silva Dias, P. L., Nobre, C., Fisch, G., Dolman, A. J., Zipser,
14 E., Garstang, M., Manzi, A. O., Fuentes, J. D., Rocha, H. R., Marengo, J., Plana-Fattori, A., Sá, L. D. A.,
15 Alvalá, R. C. S., Andreae, M. O., Artaxo, P., Gielow, R., and Gatti, L.: Cloud and rain processes in a
16 biosphere-atmosphere interaction context in the Amazon Region, *Journal of Geophysical*
17 *Research:Atmospheres*, 107, LBA 39–1–LBA 39–18, <https://doi.org/10.1029/2001JD000335>, 8072, 2002.
- 18
- 19 Sinyuk, A., Holben, B. N., Smirnov, A., Eck, T. F., Slutsker, I., Schafer, J. S., Giles, D. M., and Sorokin,
20 M.: Assessment of error in aerosol optical depth measured by AERONET due to aerosol forward scattering,
21 *Geophysical Research Letters*, 39, n/a–n/a, <https://doi.org/10.1029/2012GL053894>, 123806, 2012.
- 22
- 23 Tomasi, C.; Petkov, B.H. Calculations of relative optical air masses for various aerosol types and minor
24 gases in Arctic and Antarctic atmospheres. *Journal of Geophysical Research: Atmospheres*. 2014, 119,
25 1363–1385. <https://doi.org/10.1002/2013JD020600>
- 26
- 27 van Donkelaar, A., Martin, R. V., Brauer, M., Kahn, R., Levy, R., Verduzco, C., and Villeneuve, P. J.:
28 Global Estimates of Ambient Fine Particulate Matter Concentrations from Satellite-Based Aerosol Optical
29 Depth: Development and Application, *Environmental Health Perspectives*, 118, 2010.
- 30
- 31 van Donkelaar, A., Martin, R. V., Spurr, R. J. D., Drury, E., Remer, L. A., Levy, R. C., and Wang, J.:
32 Optimal estimation for global ground-level fine particulate matter concentrations, *Journal of Geophysical*
33 *Research: Atmospheres*, 118, 5621–5636, <https://doi.org/10.1002/jgrd.50479>, 2013.
- 34
- 35 Yamasoe, M. A. and do Rosario, N. E.: Changes in solar radiation partitioning reaching the surface due to
36 biomass burning aerosol particles in the Amazon Basin, *AIP Conference Proceedings*, 1100, 657–660,
37 <https://doi.org/10.1063/1.3117072>, 2009.
- 38
- 39 Yamasoe, M. A., Rosario, N. M. E. d., Leiva, E. A., Costa, T. S., and Braghieri, R. K.: Aerosol optical
40 properties, downward solar irradiance and Ozone concentrations measured at Humaitá, AM, during the
41 biomass burning season of 2012, in: *In: Changing chemistry in a changing world: Scientific Program*,
42 *International Commission on Atmospheric Chemistry and Global Pollution*, 2014.